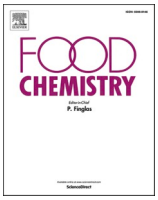
Food Chemistry 496 (2025) 146687



Contents lists available at ScienceDirect

Food Chemistry

journal homepage: www.elsevier.com/locate/foodchem





Ultrasonic agglomeration applied to *Durvillea Antarctica* and *Arthrospira platensis* flours: Effects on thermophysical properties, protein conformational changes and microstructure

Daniela Rivera-Tobar [a,*], Mario Pérez-Won [b,*], Erick Jara-Quijada [c], Luis González-Cavieres [d], Gipsy Tabilo-Munizaga [b], Roberto Lemus-Mondaca [e], Fernando Osorio-Lira [a]

[a] Department of Food Science and Technology, Universidad de Santiago de Chile, Av. Víctor Jara, 3769 Santiago, Chile
[b] Department of Food Engineering, Universidad del Bío-Bío, Av. Andrés Bello 720, Box 447, Chillán, Chile
[c] Nutrition and Dietetics, Universidad Adventista de Chile, Camino a Las Mariposas 11771, Chillán, Chile
[d] Nutrition and Dietetics, Faculty of Health Sciences, Universidad Católica del Maule, Chile
[e] Department of Food Science and Chemical Technology, Universidad de Chile, Calle Dr. Carlos Lorca 964, Santiago, Chile

ARTICLE INFO

Keywords:
ultrasonic agglomeration
cochayuyo
spirulina
thermophysical properties
microstructure

ABSTRACT

The effects of ultrasonic agglomeration (UA) on the thermophysical and structural properties of matrices based on flours from Durvillaea antarctica and Arthrospira platensis were evaluated. UA was applied under power amplitudes, times, and cycles, optimizing the processing conditions in the agglomerated matrix. The elastic modulus increased significantly under optimal UA conditions, reaching 43.08 ± 1.93 N/m^2 at 90 % power amplitude, compared to 0.051 ± 0.10 N/m^2 at 70 % power amplitude. Fractrutability increased by more than 50 %, reaching values up to 931.89 ± 23.78 N (90 % power amplitude, 25 s, 3 cycles). The protein denaturation temperature increased to 134–139 °C with UA, indicating increased thermal stability. FTIR analysis revealed a reduction in β-sheet content (from 70.9 ± 3.1 % to ~50–58 %) and an increase in α-helix structures, reflecting protein unfolding. UA is an alternative to be explored in the food industry, with potential application in the development of functional and sustainable foods.

1. Introduction

Ultrasound (US) is a promising technology in the food industry, facilitating various unit operations such as extraction, emulsification, and pasteurization (Bhargava et al., 2021; Singla & Sit, 2021). The principle of US is based on generating shear forces at the cellular level through cavitation, which can lead to cell membrane disintegration (Gavahian et al., 2020). Other physical effects, including microcurrents and shock waves, also significantly contribute to cellular damage and enhanced permeability (Cao et al., 2019; Khaire et al., 2021).

The application of US technology in food processing induces significant alterations in the chemical structures and microstructures of food components, directly impacting their functional properties. Specifically, ultrasonic treatment generates hydrogen ions and free radicals in water molecules, facilitating various chemical reactions (Cao et al., 2019; Pétrier et al., 2007). Sonomechanical effects arising from molecular agitation can profoundly modify protein structures, including chain breaks and alterations in amino acid side groups, potentially leading to transient or permanent structural changes (Su & Cavaco-Paulo, 2021). Studies on pea protein isolates have demonstrated that US can induce changes in secondary, tertiary, and quaternary protein structures, promoting aggregation and cross-linking while exposing hydrophobic groups at the surface (Cheng & Cui, 2021; Rahman & Lamsal, 2021). Ultrasound has also been shown to activate and deactivate enzymes; specific studies have focused on the inactivation of phenol peroxidase and polyphenol oxidase (Bermúdez-Aguirre et al., 2011). Zhu and Li (2019) highlighted that US facilitates the depolymerization of konjac glucomannan, a natural polysaccharide derived from the konjac tuber. Barrett et al. (2018) and Barrett and Capodieci (2019) found that ultrasonic agglomeration (UA) in wheat flour matrices enhanced structural stability. This process reduced the need for low nutritional value binders and enabled the use of larger particle sizes, thus contributing to a more appealing and natural appearance of food products.

Macroalgae (such as cochayuyo) and microalgae (such as spirulina)

* Corresponding authors.
E-mail addresses: daniela.rivera.t@usach.cl (D. Rivera-Tobar), mperez@ubiobio.cl (M. Pérez-Won).

https://doi.org/10.1016/j.foodchem.2025.146687
Received 5 May 2025; Received in revised form 14 September 2025; Accepted 6 October 2025
Available online 9 October 2025
0308-8146/© 2025 Elsevier Ltd. All rights are reserved, including those for text and data mining, AI training, and similar technologies.

have emerged as alternative protein sources of high nutritional value, with protein contents that can exceed 60 % dry weight and complete amino acid profiles (Prates, 2025). Furthermore, they present significant environmental advantages, such as low water resource demand and the capacity to capture CO_2, contributing to the sustainability of their production (Guadalupi et al., 2025). Algal proteins exhibit excellent functional properties, including solubility, emulsifying capacity, and gelling ability, making them ideal for the development of innovative, alternative, and sustainable food products (Thakur et al., 2024). The integration of algal proteins into food matrices through advanced technologies like ultrasonic agglomeration allows for the development of products with improved textural and sensory properties, as well as enhanced structural stability. This technological strategy not only boosts the utilization of alternative protein sources but also responds to the growing demand for functional and sustainable foods (Braspaiboon et al., 2022).

Ultrasonic agglomeration (UA) utilizes physical and chemical changes induced by ultrasonic waves to compact food, promoting densification and enhancing material bonding without additives. These molecular interactions, occurring under compressive pressure, form permanent bridges, resulting in compressed foods with increased mechanical stability (Barrett et al., 2021). Key UA process parameters include power amplitude, ultrasonic time, ultrasonic energy, and mechanical compression force. While vibration frequency is typically fixed (20 kHz for food), power amplitude is adjusted to control energy transmission, which governs food transformations and texture development (Rivera-Tobar et al., 2024; Barrett et al., 2018). Despite growing interest, a comprehensive understanding of UA applications in compaction and agglomeration is still needed. Therefore, the present study aimed to evaluate textural changes and their correlation with conformational alterations, thermophysical properties, and microstructure of combined cochayuyo (macroalgae) and spirulina (microalgae) flour mixes.

2. Materials and methods

2.1. Raw materials

The macroalga *Durvillaea antarctica*, known as cochayuyo in Chile, was purchased from a local market (Chillán, Ñuble Region, Chile). Cochayuyo samples were cut into small pieces (2 × 2 × 3 cm) and dried in a forced convection oven (Model 3900B, Excalibur Food Dehydrators. Sacramento, CA, USA) for 4 h at 50 °C to reach an approximate average moisture content of 20 %.; this prevented the cochayuyo pieces from sticking to the pulverizer, which was the next stage in the production of cochayuyo flour. The sample was pulverized in a high-shear mill (ZM 200, Retsch GmbH, Haan, Germany) at 6000 rpm with a 500 μm sieve mesh to obtain the cochayuyo flour (Uribe et al., 2020). Spirulina (*Arthrospira platentis)* powders were purchased from a local shop (Chillán, Ñuble Region, Chile).

2.2. Proximal composition

The moisture, protein, lipid, ash, and carbohydrate contents of cochayuyo and spirulina flours, control sample (compacted without US), and samples under the different study conditions (compacted with ultrasound, US) were measured according to the procedures described by the Association of Official Analytical Chemists (AOAC, 1991). Moisture and ash were determined using the gravimetric principle by oven drying and muffle incineration methods, respectively. The lipid content was established by the Soxhlet extraction method, the protein content by the Kjeldahl method (Baur & Ensminger, 1977), and the carbohydrate content by subtracting the sum of the percentages of protein, lipid, ash, and moisture content (Nilusha et al., 2021).

2.3. Particle size distribution

The particle size of the flours and control samples was measured with a laser scattering particle size distribution analyzer (LA-960 V2, Horiba, Kyoto, Japan). The temperature was 25 °C, and distilled water with a 1.33 refractive index was used as the dispersing medium. Data was analyzed with software (HORIBA LA-960 Instruments Inc., Irvine, CA, USA) provided by the instrument supplier and represented as mean particle size (Lu et al., 2024).

2.4. Development of agglomerated matrices based on cochayuyo and spirulina flours

The development of agglomerated matrices was conducted in two stages. First, a homogeneous mixture consisting of 30.5 % spirulina flour, 30.5 % cochayuyo flour, and 39 % of a 0.6 M NaCl solution was prepared, adjusting the total moisture content to 30 %. This specific blend ratio of macroalgae and microalgae was chosen to leverage their complementary nutritional profiles and functional properties, which can lead to enhanced protein quality and improved textural attributes in food matrices (García-Segovia et al., 2020; Priyadarshani & Rath, 2012). The inclusion of 0.6 M NaCl solution was critical, as sodium chloride plays a significant role in modulating protein-protein interactions, influencing water activity, and facilitating efficient ultrasonic energy transfer, all of which are crucial for effective agglomeration (Damodaran, 2008; Li et al., 2019).

In the second stage, the prepared mixture was placed into a rectangular mold (5 × 4 × 2 cm) within the ultrasonic agglomeration (UA) equipment (Branson 2000×). Negative control was established by applying only mechanical pressure (65 psi) via the Sonotrode descent, without activating the ultrasound. For the experimental treatments, twenty-seven distinct UA processing conditions were evaluated, varying amplitude percentages (70 %, 80 %, and 90 %), exposure times (20, 25, and 30 s), and number of cycles (3, 4, and 5). Constant pressure and a fixed vibration frequency of 20 kHz were maintained throughout these treatments (Barrett et al., 2021). The selection of these ultrasonic parameters was based on their documented influence on agglomeration efficiency and the final properties of food matrices. High power amplitude (70–90 %) are known to generate stronger cavitation effects, promoting more robust interparticle bonding and enhanced structural cohesion (Kentish & Feng, 2014). Moderate exposure times (20–30 s) were chosen to ensure optimal compactness, balancing the need for sufficient energy input with the prevention of over-processing that could negatively impact internal structure or functional properties (Chemat et al., 2017). Furthermore, the application of multiple cycles (3–5) was crucial for achieving a homogeneous distribution of ultrasonic energy, which is essential for uniform particle agglomeration, particularly in complex matrices like those derived from algae (Ashokkumar, 2011). Following agglomeration, all samples were dried in a forced convection oven (Excalibur Food Dehydrators Model 3900B) at 45 °C to achieve a final moisture content ranging from 9 % to 13 %.

2.5. Identification of secondary structures by Fourier transform infrared spectroscopy with attenuated total reflectance

Infrared spectra were measured at room temperature using Fourier transform infrared (FT-IR) equipment (Shimadzu Corporation Pte. Ltd., Kyoto, Japan) with 128 scans set at a spectral resolution of 4.0 cm^{-1}. A sample mass of 1 mg was placed on the surface of the attenuated total reflectance glass and pressed with a flat-tipped plunger until spectra with suitable peaks were produced. The spectra were between 1600 and 1700 cm^{-1} (amide I region) and exhibited temperature dependence. The resulting spectra were mathematically processed using IRsolution v.1.10 software (Creon Lab Control AG, Shimadzu Corporation Pte. Ltd., Kyoto, Japan). The amide I region (1600–1700 cm^{-1}) was analyzed by a deconvolution procedure (OriginPro 2015, OriginLab Corporation,

Northampton, MA, USA); secondary structures were quantified according to Jackson and Mantsch (1995) and reported as percentage frequency. The amide I region was evaluated to estimate the proportion of secondary structures in the control sample and UA- The FT-IR spectra analysis of the arrays of different protein secondary structures in the amide I region revealed five leading Gaussian bands located at ~1632, ~ 1649, ~ 1665, ~ 1680, and ~ 1694 cm^{-1}, which corresponded to the β-sheet, α-helix, β-turn, anti-parallel β-sheet, and intermolecular aggregates, respectively (Benelhadj et al., 2023; Shevkani et al., 2015; Zeng et al., 2020).

2.6. Thermogravimetric analysis by differential scanning calorimetry

Thermophysical parameters were obtained by differential scanning calorimetry (DSC) thermograms in the control sample and UA-treated samples. Enthalpy change of glass transition temperature (ΔH_{tg}), protein denaturation temperature (T_m), enthalpy changes of protein denaturation temperature (ΔH_{tm}), changes in specific heat (ΔC_p), and glass transition temperature (T_g) were determined by differential scanning calorimeter (DSC 7, PerkinElmer, Norwalk, CT, USA) calorimetry differential barred PerkinElmer (PE; Norwalk, CT).equipped with a low temperature cooling unit (LTC-50, Shimadzu Corporation, Kyoto, Japan). Samples (7–8 g) were placed in hermetically sealed aluminum capsules, and an empty capsule was used as a reference. The temperature program consisted of cooling from 25 to −70 °C at a rate of −10 °C/min, followed by a 2-min holding period, and then heating to 200 °C at a rate of 5 °C/min. An airtight capsule was used as a reference, and a constant N_2 flow rate of 50 mL/min was maintained. The thermograms were analyzed with the Pyres Player software to determine enthalpy (calculated from the area of the endothermic peak under the baseline), which was expressed in Joules per gram fresh weight (J/g FW) in the phase transitions, and as the glass transition and protein denaturation temperatures.

2.7. Determination of elastic modulus and fracturability

The control sample and UA-treated samples were subjected to a uniaxial compression test with a texture analyzer (TA-TX PLUS model, Texture Technologies, Scarsdale, NY, USA). Compression tests were performed with a model P75 cylindrical aluminum plate at room conditions (20 °C, 1 atm). Force calibration and sensitivity were checked with 5 kg weight, and the probe position calibrations were performed before the test. The tests were performed with a constant crosshead speed of 1 mm/s. Samples were compressed to a 75 % strain, but only the reversible domain was considered. Strain–stress curves were analyzed, and elastic modulus (N/m^2) was calculated from the slope in the elastic region (Texture Expert v.2.63 software, Stable Micro Systems Ltd., Godalming, UK). Fracturability values of samples treated with UA were obtained from the highest point of the strain-stress curve (Masavang et al., 2019).

2.8. Experimental design and optimization

The optimization of the elastic modulus (Pa), fracturability (N), and degree of denaturation (%) responses was performed using the response surface methodology. A 3^3 factorial experimental design was applied, considering the following independent variables: power amplitude (A: 70–90 %), time (B: 20–30 s), and the number of cycles (C: 3–5). The levels of each factor were defined based on preliminary studies and the operational limitations of the ultrasound system. The experimental design included factorial points at high (+1) and low (−1) levels, as well as center points (0), allowing the evaluation of linear and quadratic effects and interactions between factors. This strategy allowed for modeling and optimization of the ultrasonic agglomeration treatment conditions to maximize the evaluated properties. To describe the relationship between the factors and the response variables, a second-order statistical model (quadratic equation) was fitted, as expressed in Eq. (1):

$$Y = \beta 0 + \beta_1 A + \beta_2 B + \beta_3 C + \beta_{12} AB + \beta_{13} AC + \beta_{23} BC + \beta_{11} A^2 + \beta_{22} B^2 + \beta_{33} C^2 + \varepsilon \quad (1)$$

Where Y represents the response variable (elastic modulus, fracturability or denaturation), A is the power amplitude(%), B is the Time (s), C is the number of cycles, β_0 is the constant term, β_1, β_2, β_3 are the linear coefficients, β_{12}, β_{13}, β_{23} are the interaction coefficients, β_{11}, β_{22}, β_{33} are the quadratic coefficients and ε is the random error term.

2.9. Microstructure

Control sample and UA-treated samples had dimensions of 2 × 2 × 2 cm (height, width, and length) and were observed under an optical microscope (ODC-89 model, KERN, Balingen, Germany) without prior preparation at 200× magnification. The compacted matrices were placed on a watch glass, cut into thin uniform cross-sections with a scalpel and forceps and deposited on the copper grid sample holder (300 mesh) covered with scanning electron microscope gold film (EVO, MA10, Carl Zeiss, Jena, Germany) at 100 μm magnification. Images of the agglomerated samples were obtained by US with a Carl Zeiss confocal laser microscope (LSM 800, Carl Zeiss, Jena, Germany). The transmission of 2.5 % nominal laser power was used, along with DAPI (4,6-diamidino-2-phenylindole) at 410 nm, AF (alexa fluor) at 647 nm, and a wavelength range of 410 to 617 nm for all the analyzed samples. In addition, the samples were immersed in ZEISS immersion agent Immersol W 2010, which has a refractive index of 1334.

2.10. Statistical analysis

Results were analyzed with Minitab 19.0 statistical software to perform a multifactorial analysis of variance (ANOVA) between the study factors. The experimental design samples were run in duplicate and Fisher's LSD test (for multifactorial ANOVA without control) and Dunnett's test (including control) were used to minimize significant differences with a 95 % confidence interval.

3. Results and discussion

3.1. Characterization of flours and control matrix

Fig. 1 shows the spirulina and cochayuyo flours and the control sample flours characterized by proximate composition analysis, particle size distribution determination, DSC, and FT-IR. Moisture content ranged from 7.82 ± 0.51 % to 32.17 ± 1.57 %, ash from 9.55 ± 0.87 % to 23.91 ± 0.17 %, lipids from 0.15 ± 0.02 % to 0.76 ± 0.69 %, proteins from 66.07 ± 1.22 % to 9.98 ± 1.72 %, and carbohydrates from 12.40 ± 0.55 % to 50.57 ± 2.10 %. The proximate composition of cochayuyo and spirulina flours was comparable to findings reported by Gordalina et al. (2021) and Mateluna et al. (2020). A range of 79.49 ± 2.62 to 308.89 ± 5.61 was reported for the particle size analysis. Fig. 1b shows that the particle size distribution of the spirulina flour was unimodal with a mean size of 79.49 ± 2.62 μm. This result was similar to sizes obtained by Ahmed and Kumar (2022), who evaluated particle size distributions in high-pressure-treated spirulina. They observed a unimodal distribution curve, and a higher percentage of particles, which ranged from 2.42 to 66.9 μm. A value of 308.89 ± 5.61 μm was obtained for cochayuyo. Covacevich et al. (2024) found a higher percentage of particle size distribution that ranged from 250 to 500 μm, which was similar to the results of the present study (Fig. 1a). The FT-IR analysis provided sample ranges of 50.31 ± 0.14 % to 70.92 ± 3.10 % for β-sheet, 20.03 ± 0.18 % to 7.38 ± 2.11 % for α-helix, 13.9 ± 2.08 % to

a

	Spirulina	Cochayuyo	Control sample
Proximal composition (%)			
Moisture	7.82 ± 0.51	15.38 ± 1.56	32.17 ± 1.7
Ash	9.55 ± 0.87	23.91 ± 0.17	15.96 ± 1.18
Lipids	4.47 ± 0.47	0.15 ± 0.02	0.76 ± 0.69
Protein	66.07 ± 1.22	9.98 ± 1.72	31.49 ± 0.97
Carbohydrates	12.40 ± 0.55	50.57 ± 2.10	19.62 ± 2.46
Distribution particle size: mean size (μm)	79.49 ± 2.62	308.89 ± 5.61	219.64 ± 6.27
Fourier transform infrared spectroscopy (%)			
β-sheet	50.31 ± 0.14	60.37 ± 0.50	70.92 ± 3.10
α-helix	20.03 ± 0.18	8.63 ± 1.03	7.38 ± 2.11
B-turn	13.9 ± 2.08	10.02 ± 0.97	7.95 ± 0.64
Antiparallel β-sheet	12.99 ± 0.07	20.09 ± 0.01	11.46 ± 1.61
Differential scanning calorimetry			
ΔCp	0.66 ± 0.05	1.43 ± 0.35	1.26 ± 0.00
ΔH_{tg}	7.88 ± 0.18	10.89 ± 0.05	10.38 ± 1.08
Tg	25.11 ± 0.47	25.82 ± 0.28	26.90 ± 1.41
Tm	114.27 ± 1.35	113.1 ± 0.41	127.34 ± 0.88
ΔH_{tm}	84.18 ± 0.49	97.27 ± 0.18	63.93 ± 0.96

b

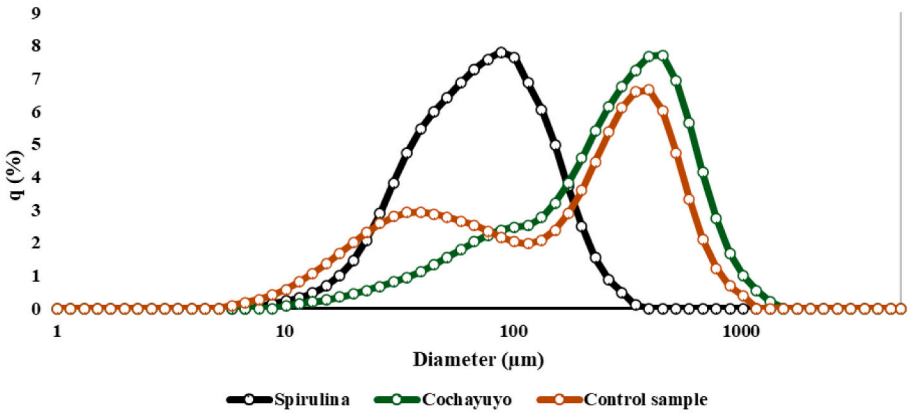


Fig. 1. a: Physicochemical characterization; b: particle size distribution of *spirulina*, *cochayuyo*, and control sample.

7.95 ± 0.64 % for β-turn, and 20.09 ± 0.01 % to 11.46 ± 1.61 % for antiparallel β-sheet. Ladjal-Ettoumi et al. (2024) reported 25.04 % of the secondary structure of the α-helix protein for spirulina, which was similar to findings of the present study. These α-helix values contributed to improved solubility, thus allowing spirulina to dissolve and mix easily with cochayuyo flour (Bai et al., 2015). The DSC analysis showed that the cochayuyo protein enthalpy of denaturation was significantly higher than for spirulina (97.27 ± 0.18 (J/g) and 84.18 ± 0.49 (J/g), respectively). This can occur because cochayuyo is a thermophilic organism, which can withstand higher temperatures, and this suggests that its proteins have advanced mechanisms to maintain structural integrity and functionality under these conditions (Farkas & Mohácsi-Farkas, 1996). In contrast, mesophilic organisms such as spirulina can have lower thermal protein stability (Sawle & Ghosh, 2011). (See Fig. 1). The keys to the treatments applied with ultrasonic agglomeration according to the operational variables based on the experimental design are found in the Table 1.

3.2. *Proximal analysis of matrices agglomerated with ultrasound*

Ultrasonic agglomeration of cochayuyo and spirulina flours produced matrices with stable proximal composition and significant differences depending on the applied power amplitude, as shown in Table 2. Increasing the ultrasonic power amplitude favored greater compaction and cohesion of the particles, which translated into increases in the thermal stability and mechanical strength of the matrix, in

Table 1
Keys to treatments applied with ultrasonic agglomeration operational variables based on experimental design.

Code	Ultrasonic agglomeration operational conditions
T1	70 % power amplitude, 20 s, 3 cycles
T2	70 % power amplitude, 20 s, 4 cycles
T3	70 % power amplitude, 20 s, 5 cycles
T4	70 % power amplitude, 25 s, 3 cycles
T5	70 % power amplitude, 25 s, 4 cycles
T6	70 % power amplitude, 25 s, 5 cycles
T7	70 % power amplitude, 30 s, 3 cycles
T8	70 % power amplitude, 30 s, 4 cycles
T9	70 % power amplitude, 30 s, 5 cycles
T10	80 % power amplitude, 20 s, 3 cycles
T11	80 % power amplitude, 20 s, 4 cycles
T12	80 % power amplitude, 20 s, 5 cycles
T13	80 % power amplitude, 25 s, 3 cycles
T14	80 % power amplitude, 25 s, 4 cycles
T15	80 % power amplitude, 25 s, 5 cycles
T16	80 % power amplitude, 30 s, 3 cycles
T17	80 % power amplitude, 30 s, 4 cycles
T18	80 % power amplitude, 30 s, 5 cycles
T19	90 % power amplitude, 20 s, 3 cycles
T20	90 % power amplitude, 20 s, 4 cycles
T21	90 % power amplitude, 20 s, 5 cycles
T22	90 % power amplitude, 25 s, 3 cycles
T23	90 % power amplitude, 25 s, 4 cycles
T24	90 % power amplitude, 25 s, 5 cycles
T25	90 % power amplitude, 30 s, 3 cycles
T26	90 % power amplitude, 30 s, 4 cycles
T27	90 % power amplitude, 30 s, 5 cycles

agreement with what has been reported in previous studies on plant and algal proteins (Barrett et al., 2021; Rivera-Tobar et al., 2024). The results of Table 2 show that the application of high power amplitude (90 %) and long times (30 s) increased the protein denaturation temperature and the elastic modulus, indicating a denser structure resistant to thermal denaturation. Furthermore, the ultrasonically processed samples showed a significant reduction in final moisture and an increase in available protein content, suggesting improved nutrient retention and technological functionality of the matrix. These findings reinforce the potential of ultrasonic agglomeration as a tool to improve the structural and nutritional quality of seaweed-based products, although further validation of these effects with advanced molecular analysis is recommended in future studies. Specifically, the proximal composition values of the control sample were moisture 32.17 ± 1.7 %, ash 15.96 ± 1.18 %, lipids 0.76 ± 0.69 %, proteins 31.49 ± 0.97 %, and 19.62 ± 2.46 % carbohydrates (Fig. 1). Table 2 shows that samples T9, T18, and T27 have proximal composition ranges of 30.12 ± 0.49 to 33.00 ± 1.35 moisture, 15.37 ± 1.46 to 17.46 ± 0.08 ash, 0.26 ± 0.01 to 0.44 ± 0.12 lipids, 31.75 ± 0.01 to 33.43 ± 1.51 proteins, and 18.55 ± 1.64 to 20.68 ± 0.61 carbohydrates; there are no significant differences ($p < 0.05$) between them. This indicated the effectiveness of applying UA because it generated the agglomeration of cochayuyo and spirulina flours while maintaining the proximal composition of the macronutrients. Ultrasonic agglomeration generated ultrasonic waves in the feed to create cavitation bubbles that caused localized points of heat and pressure. The particle surfaces liquefied and welded together to create permanent particle bridges between the spirulina and cochayuyo flours without binding additives and without modifying the proximate composition of the feed. This application is crucial for the development of innovative products with clean label formulations without additives (Rivera et al., 2024).

3.3. Identification of secondary structures by Fourier transform infrared spectroscopy of matrices agglomerated with ultrasound

The amide I region (1600–1700 cm^{-1}) was evaluated by FT-IR to determine differences in the protein secondary structure. Table 3a shows

Table 2
Proximal composition of samples under ultrasonic agglomeration conditions.

	Moisture	Ash	Lipid	Protein	Carbohydrate
T1	32.49 ± 2.29 ^{A}	16.33 ± 0.63 ^{A}	0.88±0.18 ^{A}	31.25 ±1.14 ^{A}	19.83±0.95 ^{A}
T2	33.78 ±1.73 ^{A}	16.06 ± 1.49 ^{A}	0.83 ±0.46 ^{A}	32.51 ±1.81 ^{A}	19.45±2.20 ^{A}
T3	32.56 ± 1.09 ^{A}	15.90 ± 0.62 ^{A}	0.76 ±0.20 ^{A}	32.55 ±2.61 ^{A}	19.28±1.02 ^{A}
T4	32.47± 3.42 ^{A}	15.99 ± 1.85 ^{A}	0.79 ±0.57 ^{A}	31.28 ±1.87 ^{A}	19.30±2.76 ^{A}
T5	33.83 ± 2.45 ^{A}	16.01 ± 1.26 ^{A}	0.80 ±0.35 ^{A}	32.59 ±1.15 ^{A}	19.45±1.88 ^{A}
T6	32.50 ± 1.80 ^{A}	16.12 ± 0.62 ^{A}	0.88 ±0.11 ^{A}	31.50 ±1.96 ^{A}	19.84±0.54 ^{A}
T7	32.70 ± 3.19 ^{A}	15.95 ± 1.49 ^{A}	0.77±0.46 ^{A}	32.78 ±1.72 ^{A}	19.39±2.42 ^{A}
T8	33.70 ± 1.35 ^{A}	15.78 ± 0.62 ^{A}	0.77 ±0.11 ^{A}	32.50 ±2.28 ^{A}	19.33±0.63 ^{A}
T9	35.00 ±1.35 ^{A}	15.37 ± 1.46 ^{A}	0.26 ±0.01 ^{A}	30.80 ±1.67 ^{A}	18.57±1.12 ^{A}
T10	33.36 ±2.62 ^{A}	15.98 ± 2.00 ^{A}	0.78 ±0.67 ^{A}	31.00 ±1.73 ^{A}	19.22±3.00 ^{A}
T11	32.36±2.32 ^{A}	15.95 ± 1.32 ^{A}	0.82 ±0.39 ^{A}	32.15 ±1.60 ^{A}	19.31±1.85 ^{A}
T12	33.34 ±1.41 ^{A}	16.23 ±0.62 ^{A}	0.85 ±0.21 ^{A}	31.45 ±1.57 ^{A}	19.72±0.55 ^{A}
T13	33.85 ±2.75 ^{A}	15.99 ± 1.71 ^{A}	0.79 ±0.56 ^{A}	32.79 ±1.26 ^{A}	19.37±2.57 ^{A}
T14	31.67 ±2.04 ^{A}	15.67 ±0.62 ^{A}	0.76 ±0.19 ^{A}	32.28 ±2.43 ^{A}	19.22±0.63 ^{A}
T15	33.67 ±1.43 ^{A}	15.90 ±2.06 ^{A}	0.79 ±0.61 ^{A}	30.99 ±1.56 ^{A}	19.14±2.71 ^{A}
T16	33.55 ± 2.66 ^{A}	16.35 ±0.50 ^{A}	0.81 ±0.31 ^{A}	32.33 ±1.71 ^{A}	19.62±1.80 ^{A}
T17	32.44 ± 2.04 ^{A}	15.97 ±0.61 ^{A}	0.85 ±0.10 ^{A}	31.39 ±1.96 ^{A}	19.67±0.94 ^{A}
T18	30.12 ± 0.69 ^{A}	17.50 ±0.06 ^{A}	0.38 ±0.04 ^{A}	34.29 ±0.27 ^{A}	17.71±1.06 ^{A}
T19	33.51 ± 3.06 ^{A}	15.95 ±1.27 ^{A}	0.75 ±0.75 ^{A}	32.58 ±2.37 ^{A}	19.12±0.62 ^{A}
T20	32.08 ±3.06 ^{A}	16.18 ±0.65 ^{A}	0.78 ±0.78 ^{A}	31.02 ±1.88 ^{A}	19.30±2.62 ^{A}
T21	33.95 ± 1.35 ^{A}	16.06 ±1.68 ^{A}	0.81 ±0.81 ^{A}	32.51 ±1.17 ^{A}	19.57±1.89 ^{A}
T22	34.09 ± 1.46 ^{A}	15.62 ±0.62 ^{A}	0.85 ±0.85 ^{A}	31.61 ±1.96 ^{A}	19.83±0.86 ^{A}
T23	33.12 ± 2.32 ^{A}	15.89 ±2.12 ^{A}	0.80 ±0.80 ^{A}	32.97 ±1.54 ^{A}	19.53±2.48 ^{A}
T24	34.06 ± 2.58 ^{A}	16.35 ±0.57 ^{A}	0.78 ±0.78 ^{A}	31.89 ±1.73 ^{A}	19.44±0.64 ^{A}
T25	32.65 ± 1.34 ^{A}	15.89 ±0.69 ^{A}	0.48 ±0.48 ^{A}	31.18 ±1.81 ^{A}	17.75±0.98 ^{A}
T26	32.68 ± 2.44 ^{A}	15.83 ±1.72 ^{A}	1.17 ±1.17 ^{A}	32.50 ±1.70 ^{A}	20.43±0.42 ^{A}
T27	30.32 ± 0.35 ^{A}	16.95 ±0.23 ^{A}	0.30 ±0.30 ^{A}	31.75 ±0.01 ^{A}	20.68±0.61 ^{A}

The first capital letters (A, B, and C) indicate significant differences in amplitudes according to ANOVA analysis and Fisher's test. Samples without (*) are significantly different from the control sample according to Dunnett's test.

the percentages of the relative proportions of secondary structures of the control sample and samples treated under different UA conditions. There was a significant decrease in the percentage of the relative proportion of β-sheet secondary structure under the T19, T20, T22, T25, and T26 treatments compared with other treatments with 70 % and 80 % power amplitude. A relative proportion for β-sheet of 70.92 ± 3.10 % was obtained in the control sample, and samples treated with UA were approximately 50 % to 58 %. This decrease in β-sheet was also observed in Vela et al. (2023) when applying US to tef (*Eragrostis tef*) flour in which β-sheet decreased by 12.8 %. This occurred due to a US-caused dissociation of the protein secondary structure, which made the hydrogen bonds holding the β strands together weaken or break, and resulted in a loss of organized β-sheet conformation (Eze et al., 2022). In

Table 3
a) Relative proportion of secondary protein structures; b) elastic modulus (N/m^2); c fracturability in samples under different ultrasonic agglomeration conditions.

	a) Relative proportion of secondary protein structures				b)	c)
	β-Sheet	*α-helix*	*β-Turn*	*Antiparallel β-sheet*	*Elastic modulus (N/m^2)*	*Fracturability (N)*
T1	55.27 ± 3.05 ^{A,a,A}	8.75 ± 1.33 ^{A,a,A*}	8.29 ± 1.17 ^{A,a,AB*}	24.94 ± 1.59 ^{A,a,AB}	0.51 ± 0.10 $^{A\ a\ A\ *}$	187,03 ± 42,44 ^{AaA*}
T2	57.1 ± 0.17 ^{A,a,A}	10.61 ± 0.65 ^{A,a,A*}	9.39 ± 0.19 ^{A,a,AB*}	22.15 ± 0.02 ^{A,a,AB}	0.28 ± 0.11 $^{A\ b\ A\ *}$	174,00 ± 19,18 ^{AaA*}
T3	56.48 ± 1.92 ^{A,a,A}	8.54 ± 1.92 ^{A,a,A*}	8.36 ± 0.43 ^{A,a,AB*}	25.78 ± 0.62 ^{A,a,AB}	2.04 ± 0.74 $^{A\ c\ B\ *}$	77,64 ± 5,52 ^{AaA*}
T4	56.68 ± 0.71 ^{A,a,A}	11.88 ± 0.33 ^{A,a,A*}	7.95 ± 1.43 ^{A,a,A*}	21.95 ± 0.00 ^{A,a,A}	2,21 ± 0.89 $^{A\ a\ A\ *}$	414,27 ± 21,90 ^{AaB*}
T5	58.05 ± 0.71 ^{A,a,A}	12.76 ± 0.33 ^{A,a,A*}	9.64 ± 1.43 ^{A,a,A*}	20.00 ± 0.00 ^{A,a,A}	0.64 ± 0.26 $^{A\ b\ A\ *}$	221,26 ± 45,90 ^{AaB*}
T6	57.02 ± 0.60 ^{A,a,A}	10.10 ± 0.32 ^{A,a,A*}	11.04 ± 0.57 ^{A,a,A*}	22.53 ± 0.75 ^{A,a,A}	2.56 ± 0.69 $^{A\ c\ B\ *}$	170,42 ± 32,56 ^{AaB*}
T7	55.24 ± 0.79 ^{A,a,A}	13.65 ± 0.03 ^{A,a,A*}	7.31 ± 0.12 ^{A,a,B*}	24.56 ± 0.43 ^{A,a,B}	2.42 ± 1.35 $^{A\ a\ A\ *}$	244,54 ± 32,97 ^{AaB*}
T8	56.8 ± 1.54 ^{A,a,A}	10.43 ± 0.03 ^{A,a,A*}	7.95 ± 0.50 ^{A,a,B*}	23.34 ± 0.19 ^{A,a,B}	3.44 ± 1.04 $^{A\ b\ A\ *}$	163,57 ± 34,11 ^{AaB*}
T9	53.50	10,93 ± 0.30 ^{A,a,A*}	7.32 ± 0.11 ^{A,a,B*}	27.42 ± 0.77 ^{A,a,B}	3.62 ± 0.40 $^{A\ c\ B\ *}$	463,00 ± 49,71 ^{AaB*}
T10	56.91 ± 2.01 ^{A,a,A*}	9.48 ± 2.74 ^{A,a,A*}	6.89 ± 0.61 ^{A,ab,A*}	25.15 ± 1.23 ^{A,a,A}	3.93 ± 0.41 $^{A\ a\ A\ *}$	475,32 ± 27,25 ^{AaA}
T11	54.21 ± 0.81 ^{AB,b,A*}	12.25 ± 1.34 ^{A,b,A}	9.11 ± 2.78 ^{A,a,A*}	25.02 ± 0.63 ^{A,a,A}	6.91 ± 0.72 $^{A\ a\ B\ *}$	388,41 ± 44,71 ^{BbA}
T12	54.29 ± 3.70 ^{A,b,A*}	13.00 ± 3.18 ^{B,b,A}	6.96 ± 0.74 ^{B,b,A*}	23.99 ± 1.58 ^{A,a,A}	2.28 ± 0.69 $^{A\ a\ A\ *}$	572,38 ± 31,80 ^{BcA}
T13	55.88 ± 0.11 ^{A,a,A}	12.16 ± 0.15 ^{A,a,A*}	8.10 ± 0.22 ^{A,ab,A*}	23.56 ± 0.19 ^{A,a,A}	2.51 ± 0.63 $^{A\ b\ A\ *}$	188,25 ± 20,39 ^{AaB}
T14	53.13 ± 0.58 ^{AB,b,A}	13.6 ± 0.08 ^{A,b,A}	9.21 ± 0.03 ^{A,a,A*}	23.05 ± 0.47 ^{A,a,A}	3.08 ± 1.21 $^{A\ b\ B\ *}$	214,94 ± 53,00 ^{BbB}
T15	54.21 ± 0.65 ^{A,b,A}	14.90 ± 0.72 ^{B,b,A}	6.00 ± 0.16 ^{B,b,A*}	22.88 ± 0.09 ^{A,a,A}	2.32 ± 0.80 $^{A\ b\ A}$	517,32 ± 49,10 ^{BcB}
T16	55.77 ± 1.12 ^{A,a,A*}	11.21 ± 1.58 ^{A,a,A*}	7.52 ± 0.05 ^{A,ab,A*}	23.49 ± 1.65 ^{A,a,A}	1.96 ± 0.49 $^{A\ b\ A\ *}$	513,29 ± 55,67 ^{AaA}
T17	55.67 ± 0.57 ^{AB,b,A*}	12.32 ± 1.52 ^{A,b,A}	7.42 ± 0.03 ^{A,a,A*}	25.08 ± 3.02 ^{A,a,A}	3.30 ± 0.97 $^{A\ b\ B\ *}$	224,45 ± 39,76 ^{BbA}
T18	54.86 ± 0.48 ^{A,b,A*}	12.70 ± 0.48 ^{B,b,A}	6.18 ± 0.05 ^{B,b,A*}	27.02 ± 1.39 ^{A,a,A}	2.03 ± 0.65 $^{A\ b\ A}$	503,66 ± 35,42 ^{BcA}
T19	52.18 ± 1.35 ^{B,a,A}	12.24 ± 1.51 ^{A,a,A*}	7.50 ± 1.02 ^{A,a,A*}	27.10 ± 0.35 ^{B,a,A}	1.73 ± 0.56 $^{B\ a\ A\ *}$	263,28 ± 38,92 ^{BaA}
T20	55.79 ± 3.16 ^{B,a,A}	13.00 ± 2.11 ^{A,a,A}	7.74 ± 0.65 ^{A,a,A*}	22.08 ± 0.96 ^{A,a,A}	2.09 ± 0.59 $^{B\ a\ A\ *}$	210,04 ± 23,35 ^{BbA}
T21	52.16 ± 0.25 ^{A,a,A}	12.29 ± 0.68 ^{B,a,A}	7.24 ± 0.01 ^{AB,a,A*}	29.21 ± 0.95 ^{A,a,A}	43.08 ± 1.93 $^{B\ a\ B}$	260,67 ± 33,69 ^{CbA}
T22	51.01 ± 1.69 ^{B,a,A}	13.05 ± 0.41 ^{A,a,B*}	8.22 ± 0.00 ^{A,a,A*}	27.22 ± 0.00 ^{B,a,A}	2.07 ± 0.45 $^{B\ a\ A\ *}$	931, 89 ± 23,78 ^{BaB}

Table 3 (*continued*)

	a) Relative proportion of secondary protein structures				b)	c)
	β-Sheet	*α-helix*	*β-Turn*	*Antiparallel β-sheet*	*Elastic modulus (N/m^2)*	*Fracturability (N)*
T23	52.03 ± 0.31 ^{B,a,A}	14.55 ± 1.61 ^{A,a,B}	7.44 ± 0.23 ^{A,a,A*}	24.52 ± 1.48 ^{A,a,A}	2.94 ± 0.52 $^{B\ a\ A\ *}$	281,75 ± 30,10 ^{BbB}
T24	53.60 ± 0.15 ^{A,a,A}	15.31 ± 0.64 ^{B,a,B}	7.92 ± 0.35 ^{AB,a,A*}	22.43 ± 0.21 ^{A,a,A}	8.93 ± 4.72 $^{B\ a\ B\ *}$	336,88 ± 26,51 ^{CbB}
T25	52.52 ± 2.11 $^{B,\ a,\ A}$	12.59 ± 0.88 ^{A,a,A*}	8.60 ± 0.04 ^{A,a,A*}	26.45 ± 2.01 ^{B,a,A}	21.46 ± 7.08 $^{B\ b\ A\ *}$	513,72 ± 20,54 ^{BaB}
T26	51.92 ± 2.11 ^{B,a,A}	11.56 ± 0.78 ^{A,a,A}	8.47 ± 0.04 ^{A,a,A*}	27.28 ± 2.02 ^{A,a,A}	19.60 ± 12.04 $^{B\ b\ A\ *}$	677,09 ± 23,61 ^{BbB}
T27	55.83 ± 1.29 ^{A,a,A}	12.40 ± 0.05 ^{B,a,A}	7.04 ± 1.56 ^{AB,a,A*}	23.83 ± 0.44 ^{A,a,A}	25.84 ± 2.96 $^{B\ b\ B}$	580,24 ± 44,43 ^{CbB}

The first capital letters indicate significant differences in amplitudes. Lowercase letters indicate significant differences between the number of ultrasonic aggregation cycles. The second capital letters indicate differences between ultrasonic aggregation times. Obtained by ANOVA and Fisher's post hoc test. Samples without * are significantly different from the control sample. Obtained by Dunnett's test.

general, the application of US in food matrices exposes the internal sulfhydryl and hydrophobic groups of proteins, thus unfolding the protein secondary structures (Cheng & Cui, 2021; Rahman & Lamsal, 2021; Rostamabadi et al., 2023). The relative proportion percentage of α-helix increased significantly under UA conditions in the T12, T15, T18, T21, T24, and T27 treatments. This happened because US provides the sonolysis effect of polar molecules by generating free radicals and reactive species (superoxide), thus causing oxidation by reducing sulfhydryl groups and conformational changes in the protein secondary and tertiary structure by breaking non-covalent bonds (Solomonov et al., 2024). The antiparallel β-sheet structure increased under the T19 and T25 treatments with 27.1 ± 0.35 % and 26.4 ± 2.01 %, respectively; this concurs with Martínez-Velasco (2018), who used US in broad bean protein (*Vicia faba* L.) at the same 20 kHz frequency used in the present study.

Infrared spectroscopy (FT-IR) analysis of ultrasonically agglomerated matrices reveals significant changes in protein secondary structure, evidenced by shifts in the amide I region (1600–1700 cm^{-1}) (Fig. S1), which correspond primarily to vibrations of C═O and N—H bonds associated with β-sheets and α-helices (Barrett et al., 2021; Rivera-Tobar et al., 2024). Ultrasonic treatment favored a decrease in the proportion of β-sheets and a relative increase in the α-helix, suggesting a partial unfolding and structural rearrangement of the proteins (Quian et al., 2023). These vibrational changes reflect the breaking of internal hydrogen bonds and the exposure of hydrophobic groups, facilitating new intermolecular interactions and the formation of more compact and stable networks (Wang et al., 2024). Ultrasonic agglomeration also induced shifts in FTIR peaks associated with the formation of stronger hydrogen bonds and the reorganization of hydrophobic forces, which translates into increased thermal and mechanical strength of the matrix. In agreement, the manuscript results show significant increases in the elastic modulus (up to 80 %) and fracturability (more than 50 %) under optimal power amplitude and cycle conditions, confirming that ultrasonic compaction improves the cohesion and structural stiffness of the matrix. These effects are supported by the literature, which attributes the improved mechanical and thermal properties to the reorganization of non-covalent bonds and the exposure of hydrophobic domains, promoted by ultrasonic cavitation (Sun et al., 2023). Taken together, the results demonstrate that infrared spectroscopy is a key tool to demonstrate the molecular changes induced by ultrasonic agglomeration and

their impact on the technological functionality of matrices based on macro and microalgae (Chen et al., 2022).

3.4. Thermogravimetric analysis by differential scanning calorimetry of matrices agglomerated with ultrasound

Fig. 2 shows the changes in the thermophysical parameters of flour mixes treated by UA based on the thermograms obtained by DSC. The thermophysical parameters for the UA-treated flour blends were calorific capacity (ΔC_p), glass transition temperature (T_g), enthalpy change of glass transition temperature (ΔH_{Tg}), protein denaturation temperature (T_m), and enthalpy changes of protein denaturation temperature (ΔH_{Tm}). As the power amplitude increased to 70 %, 80 %, and 90 % in the UA treatment, the ΔC_p values showed a gradually increasing trend with significant differences between the 80 % and 90 % power amplitude treatments. This indicates that there is a change in the thermal capacity of the samples treated with UA at higher power amplitude values because samples are more agglomerated at higher power amplitudes (Fig. 2). Barrett et al. (2021) also observed a change in the thermal stability of a model system of wheat flour agglomerated by the US. In samples with 4 UA cycles, T17, T20, T23, and T26, the ΔC_p (Jg^{-1}) values decreased by 0.87 ± 1.02, 1.06 ± 0.28, 0.81 ± 0.21, and 0.64 ± 0.31, respectively, and protein T_m increased. As the number of UA cycles applied to the samples increased, more intramolecular bonds were formed, which resulted in samples that needed more thermal energy for protein denaturation to occur. Pereira et al. (2018) performed a thermogravimetric analysis by DSC in a spirulina protein extract and reached a T_m value between 96.7 and 107 °C. In the present study, UA-treated samples had higher T_m values that were between 122 and 139 °C because samples contained spirulina and cochayuyo and were agglomerated.

There is no significant dependence of UA time on ΔC_p, but it was generally higher at 30 s than 20 s. at longer US times, UA-treated samples had more vibrational energy, thus increasing the molecular rearrangement with new interactions, which changed their thermal response when the samples were subjected to a thermal flow for more time. The variability of the glass transition temperature did not vary significantly in UA-treated samples. However, ΔH_{Tg} significantly increased at different power amplitude levels (70 %, 80 %, and 90 %). The number of cycles and different times applied to the UA-treated samples showed no differences for ΔH_{Tg}. Specifically, samples T22, T23, T24, T25, T26, and T27 had significantly lower ΔH_{Tg} (Jg^{-1}) values of 17.64 ± 0.78, 18.40 ± 0.87, 14.10 ± 0.22, 15.65 ± 0.51, 13.28 ± 0.98, and 17.25 ± 0.99, respectively. This means that the samples exhibited a change in heat flow absorption because they were more agglomerated than the other samples. Gürenken et al. (2015) demonstrated the effects of high-power amplitude US on cell disruption and examined the thermal properties of microalgae such as spirulina. These authors found that increasing the power amplitude of the US application decreased ΔH_{Tg}, which concurs with the present study.

The T_m value significantly increased with the UA-treated samples compared with the control sample. The T3 treatment showed a 5 % increase in T_m values ; this behavior was maintained in samples in which 80 % and 90 % power amplitudes of were applied. Furthermore, there was no significant difference between the different number of applied cycles (3, 4, and 5) in samples with 90 % power amplitude; there was protein denaturation in the samples with only three UA cycles. For times used in the UA process, it was necessary to apply 30 s to increase the protein denaturation temperature because the cavitation bubbles generated by the US treatment can alter the protein intramolecular bonds and their secondary structures (Zeller et al., 2013).

The ΔH_{Tm} values in samples with both 70 % and 90 % power amplitude were significantly higher than the control sample because applying UA induced an alteration of the hydrogen bonds and hydrophobic interactions in the sample protein structure.; this leads to a change in the protein secondary structure and alters the thermophysical parameters (Barba et al., 2015). In other words, there is a partial unfolding of the proteins to expose the hydrophobic groups with a more thermostable conformation and generate the need for more energy to denature the proteins in the samples (Purdi et al., 2023). As for the time involved in the process, the T10, T13, T16, T19, T22, and T25 treatments showed significant differences in ΔH_{Tm} values in samples with 70 % power amplitude, given that power amplitude was a predominant factor in the thermal stability of the UA-treated samples. The number of applied UA cycles showed no significant differences between 4 and 5 cycles. Therefore, to exert a change in the thermal stability of UA-treated samples, only the 3 and 4 cycle conditions need to be applied. It was determined that applying UA to the samples produced significant changes in ΔH_{Tm} at 20 s, given that the predominant study factor was the power amplitude percentage. This phenomenon was also observed for fracturability and elastic modulus in the values from the UA-treated samples (see Table 3). Table S1 shows the statistical variability of the physical parameters of the UA-treated samples.

3.5. Elastic modulus and fracturability of ultrasonic agglomerated samples

Table 3 (a and c) indicates the values for elastic modulus and fracturability of the UA-treated samples. Values for elastic modulus ranged from 0.51 ± 43.88 N/m^2. Samples with 90 % power amplitude were significantly different compared with other treatments, and elastic modulus values increased by 80 %. No differences were found between samples for the number of applied cycles. Applied processing times were significantly different between 20 and 25 s. Fracturability values ranged from 77.64 ± 5.52 (N) to 931.89 ± 23.78 (N). Fracturability increased at 80 % power amplitude onwards compared with the control sample. Agglomerated samples had a significant increase in fracturability values after four cycles. Significant differences were observed from 25 s onwards for the applied times.

The predominant study factor was the power amplitude percentage applied to the samples, which increased elastic modulus and fracturability values. Some authors, such as Barrett et al. (2021) and Mo et al. (2019), studied the application of UA in wheat flour and macroalgal biomass. They determined that the degree of agglomeration in food matrices increased as the percentage of power amplitude increased. This phenomenon occurs because the integrated agglomeration energy in food matrices is proportional to the percentage of maximum power amplitude applied by the sonotrode (Shen et al., 2022). This implies that ultrasonic waves with a higher power amplitude percentage can physically bind the matrix particles and create more compact and robust structures (Rivera et al., 2024); this leads to increased elastic modulus and fracturability values. Therefore, the optimal conditions were 90 % power amplitude, 20 s, and 5 cycles, which showed an elastic modulus value 43.08 ± 1.93 (N/m^2). The best conditions for fracturability were 90 % power amplitude, 25 s, and 3 cycles with a value of 931.89 ± 23.78 (N).

3.5.1. Effect of ultrasonic aggregation on spirulina and cochayuyo flours

Response Surface Analysis.

A response surface methodology (RSM) was applied to evaluate the effect of three independent factors—ultrasonic power amplitude (A), Time (B), and number of cycles (C)—during the ultrasonic agglomeration process in food matrices composed of cochayuyo and spirulina. The response variables analyzed were elastic modulus, fracturability, and degree of denaturation. The experimental design allowed for simultaneous modeling and optimization of these responses using advanced statistical tools such as analysis of variance (ANOVA), Pareto charts, main effects plots, and three-dimensional response surfaces, facilitating the identification of optimal operating conditions within the experimental space evaluated. The regression model fitted for the response variables was as follows:

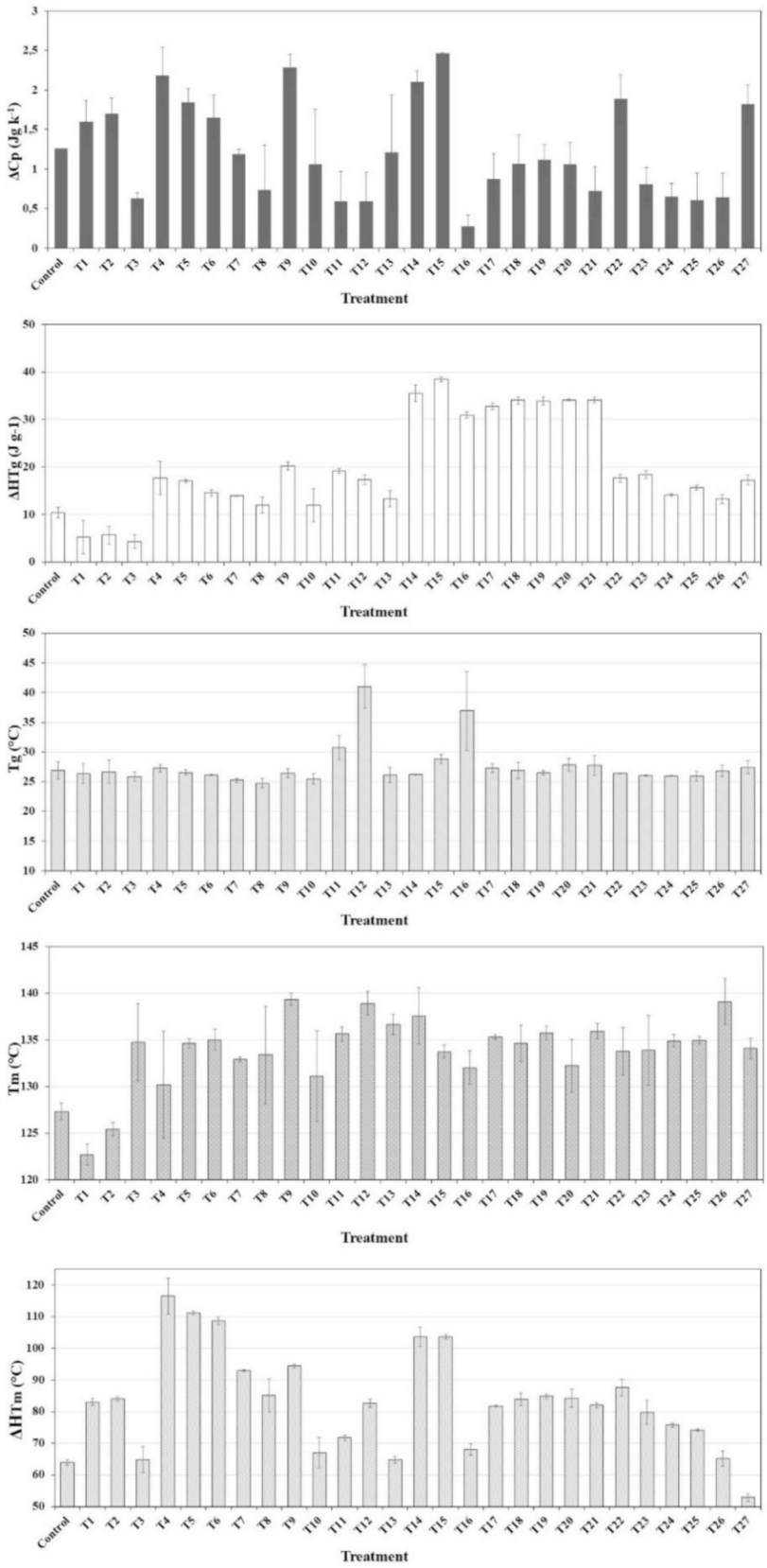


Fig. 2. Thermophysical parameters: ΔC_p :Changes in calorific capacity; ΔH_{tg} :enthalpy change of glass transition temperature; T_g:glass transition temperature; T_m :protein denaturation temperature; ΔH_{tm}: enthalpy changes of protein denaturation temperature.

$$\text{Elastic modulus} = -1,99+6,13\,A+1,14B+2,99C+4,94A^2+1,10AB +4,12\,AC+5,12B^2-2,98\,BCE+2,59C^2$$

$$\text{Fracturability} = 324,19+107,77\,A+70,83B-13,86C-56,94A^2 +50,38AB-33,03\,AC-3,43B^2+24,19\,BCE+116,82\,C^2$$

$$\text{Tm} = 135,66+1,47\,A+1,31B+1,72C-1,58A^2-1,57AB-1,91\,AC -0,69B^2-0,99\,BCE-0,16\,C^2$$

In the analysis of the variable's elastic modulus, fracturability, and degree of Tm, the models obtained using RSM showed varying levels of fit. For the elastic modulus, the model presented a coefficient of determination R^2 = 61.01 % and an adjusted R^2 = 40.38 %, indicating a moderate fit. The analysis of variance (ANOVA) revealed that ultrasonic power amplitude was the only statistically significant factor (p = 0.0032), while the AC interaction (power amplitude × cycles) and the quadratic terms showed trends close to significance. In the case of fracturability, the model explained an R^2 = 45.03 % and an adjusted R^2 = 15.93 %, demonstrating limited predictive capacity. Only power amplitude was statistically significant (p = 0.0216), suggesting a predominant effect of this factor on the mechanical strength of the system. Finally, the model corresponding to the degree of Tm presented the best fit among the three responses, with an R^2 = 64.90 % and an adjusted R^2 = 46.31 %. In this case, the factors power amplitude (p = 0.0328), number of cycles (p = 0.0146), and the AC interaction (p = 0.0245) were statistically significant, reflecting a joint influence of the sonication parameters on the structural modification of the proteins. The ANOVAs are presented below (Table 4).

The analyses performed allowed a comprehensive evaluation of the influence of ultrasonic power amplitude. Time. and number of cycles on the mechanical and structural properties of food matrices composed of cochayuyo and spirulina. Through three key response variables: elastic modulus. Fracturability. and degree of protein Tm. For the elastic modulus. The Pareto diagram showed that power amplitude was the factor with the greatest positive impact. This trend was confirmed by the main effects plots. Where a sustained increase in modulus was observed as power amplitude increased. Indicating greater compaction and reorganization of the structural network as a result of the mechanical effect of ultrasonic cavitation. Furthermore, the response surfaces revealed a positive interaction between power amplitude and number of cycles. Suggesting a favorable synergistic effect in the generation of a stiffer and more cohesive matrix. The optimal condition for maximizing this property was obtained with power amplitude = 1.0. time = −1.0. and cycles = 1.0. reaching an estimated value of 24.63 units. Regarding

Table 4
Analysis of Variance for Elastic Modulus, Fracturability, and Denaturation, respectively.

Elastic Module					
Source	Sum of Squares	Df	Mean Square	F-Ratio	*P*-Value
A: Amplitude	675.894	1	675.894	11.76	0.0032
B: Time	23.5756	1	23.5756	0.41	0.5304
C: Cycles	160.802	1	160.802	2.80	0.1127
AA	146.356	1	146.356	2.55	0.1289
AB	14.52	1	14.52	0.25	0.6216
AC	203.363	1	203.363	3.54	0.0772
BB	157.423	1	157.423	2.74	0.1162
BC	106.803	1	106.803	1.86	0.1906
CC	40.2141	1	40.2141	0.70	0.4145
Total error	976.892	17	57.4642		
Total (corr.)	2505.84	26			

Fracturability.					
Source	*Sum of Squares*	*Df*	*Mean Square*	*F-Ratio*	*P-Value*
A: Amplitude	209,046.	1	209,046.	6.40	0.0216
B: Time	90,298.3	1	90,298.3	2.76	0.1147
C: Cycles	3455.58	1	3455.58	0.11	0.7489
AA	19,456.0	1	19,456.0	0.60	0.4508
AB	30,451.7	1	30,451.7	0.93	0.3478
AC	13,087.8	1	13,087.8	0.40	0.5351
BB	70.498	1	70.498	0.00	0.9635
BC	7022.84	1	7022.84	0.22	0.6487
CC	81,884.6	1	81,884.6	2.51	0.1317
Total error	555,181.	17	32,657.7		
Total (corr.)	1.00995E6	26			

Tm.					
Source	*Sum of Squares*	*Df*	*Mean Square*	*F-Ratio*	*P-Value*
A: Amplitude	38.72	1	38.72	5.40	0.0328
B: Time	30.6806	1	30.6806	4.28	0.0542
C: Cycles	53.045	1	53.045	7.40	0.0146
AA	14.9363	1	14.9363	2.08	0.1672
AB	29.4533	1	29.4533	4.11	0.0587
AC	43.7008	1	43.7008	6.09	0.0245
BB	2.89352	1	2.89352	0.40	0.5338
BC	11.8008	1	11.8008	1.65	0.2168
CC	0.155741	1	0.155741	0.02	0.8846
Total error	121.917	17	7.17158		
Total (corr.)	347.303	26			

fracturability. The fitted model again showed a clear dominance of power amplitude as the main factor. as reflected in the Pareto diagram. The main effects plots showed that power amplitude and time favor an increase in fracturability. Likely due to the reinforcement of intermolecular interactions and the generation of denser and more brittle structures. However, the response surfaces indicated that low levels of cycles combined with high power amplitude and time values optimize this property. Which could be related to a less homogeneous texture that is more susceptible to fracture under stress. The optimal condition for this variable was obtained with power amplitude = 1.0. time = 1.0. and cycles = −1.0. reaching an estimated maximum fracturability of 632.30 units. Regarding the degree of Tm. The results indicated that the number of cycles and the interaction between power amplitude and cycles (AC) were the most relevant effects. The main effects graphs showed a progressive increase in Tm with increasing any of the three factors evaluated. While the response surfaces displayed a positive synergy between power amplitude and cycles. Which can be attributed to the intensification of the physicochemical stress induced by ultrasonic treatment. Promoting the exposure of hydrophobic groups and the rupture of tertiary structures. The optimal condition was set at power amplitude = −0.573. time = 0.873. and cycles = 1.0. predicting a maximum Tm value of 137.48 units. The main effects Pareto diagrams are presented in Fig. 3. and the response surface graphs in Fig. 4. Finally, a multiple desirability function was applied with the aim of identifying an operating condition that would allow the three responses to be maximized simultaneously. The optimal combination was power amplitude = 1.0. time = 1.0. and cycles = 1.0. under which the following values were estimated: elastic modulus: 23.15. fracturability: 586.92. Tm: 133.25. with an overall desirability of 0.586. This point represents the best functional compromise between the structural and

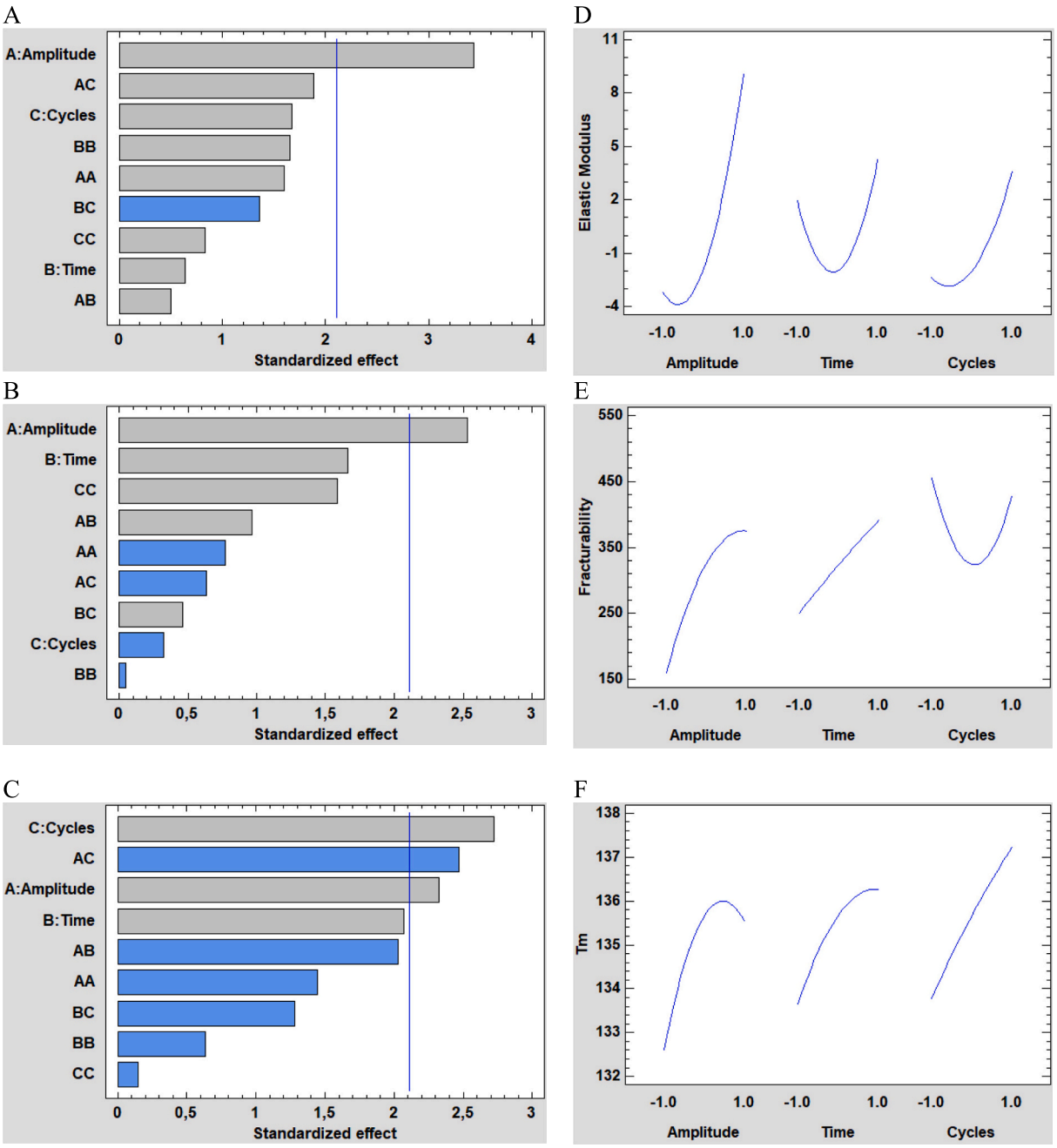


Fig. 3. Pareto diagram (A, B and C), and diagram of main effects (D, E and F) for elastic modulus Fracturability and Tm, respectively.

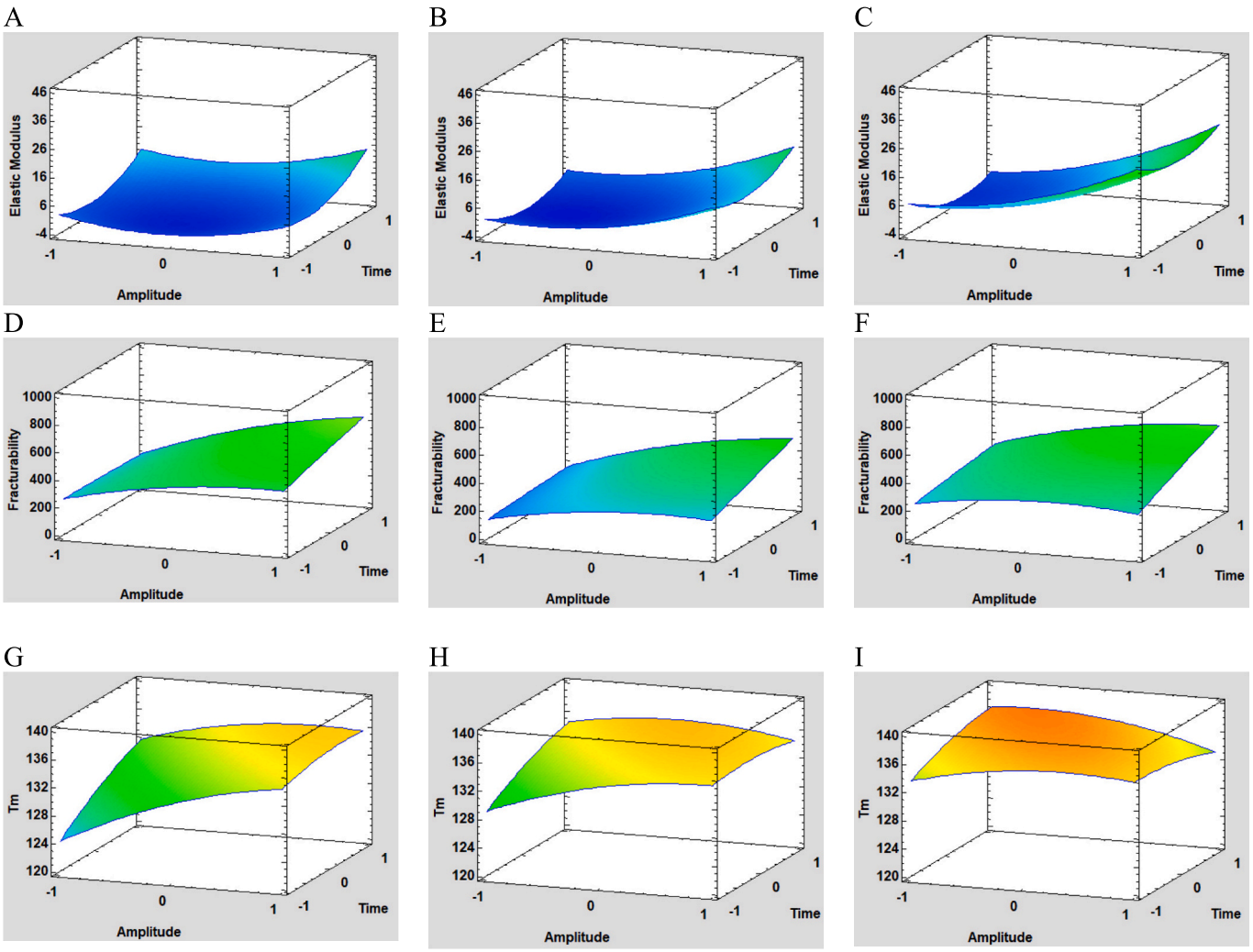


Fig. 4. Response surface plots for levels −1, 0 and 1 respectively for elastic modulus (A, B and C), fracturability (D, E and F), and Tm (G, H and I).

mechanical properties of the treated system. Being highly relevant for the design of food matrices with controlled textural characteristics and partially modified protein structures. Suitable for applications in innovative products of plant or mixed origin.

3.6. *Microstructural changes*

Different types of microscopy were used to analyze the effects of UA. Optical microscopy revealed the interaction between the cochayuyo and spirulina flour mix (Fig. 5a). Both scanning electron and confocal microscopy revealed the surface structure of the samples when UA was applied. In the control sample (Fig. 5b), the scanning electron microscopy microstructure images indicated high porosity with a heterogeneous flour distribution. One section revealed small cochayuyo flakes, whereas the spirulina flour was more homogeneously distributed in the sample. Confocal microscopy images showed that the two flours seemed to be irregularly agglomerated (Fig. 5c). The T1 treatment revealed a slight change in the microstructure with the surface becoming less rough and smoother surface areas appearing in small sections of the matrix (Fig. 5d). However, more pronounced changes were noted with 90 % power amplitude treatments (Figs. 5h, k) in which a significant portion of the sample showed smoother sections and more aggregated flours for a homogeneous structure. As for the different cycles (3 and 5) at 90 % power amplitude, no significant differences were observed in the microstructure; this substantial change was attributed to the severity of the processing, as pointed out by Barrett et al. (2021). These changes were also reflected in the elastic modulus and fracturability of the samples in which higher US power amplitude was correlated with higher values. Microstructural analysis showed greater cohesion between cochayuyo and spirulina flours and a smoother surface. The UA-treated samples showed interconnected bridges after processing, which indicated that the particles were fully integrated in a continuous network with a higher treatment power amplitude. Consequently, transformations occurred in the cochayuyo and spirulina flour particle systems through the minimal temperature rise caused by particle cavitation by US. Other authors have determined that molecular transformations, such as protein denaturation (Su & Cavaco-Paulo, 2021) and swelling and rupture of starch granules (Yu et al., 2013), have occurred when applying US and has led to the formation of continuous starch-protein networks (Fennema, 1996).

Confocal microscopy images are illustrated in Figs.5c, f, i, and l with a 3D perspective. All samples exhibited autofluorescence on their own. The control sample and T1 treatment revealed greater porosity in their structures compared with samples agglomerated at 90 % power amplitude and showed more compact aggregation. Under different UA conditions and compared with the control sample, different behaviors were observed in cochayuyo and spirulina flours. Spirulina flour was more abundantly distributed in the UA-treated samples than cochayuyo flour because spirulina flour has a higher solubility than cochayuyo flour (Caballero et al., 2021; Larrosa et al., 2018). Rodríguez De Marco et al. (2014) identified structural changes in wheat flour paste when adding spirulina and noted that the higher spirulina content resulted in a more

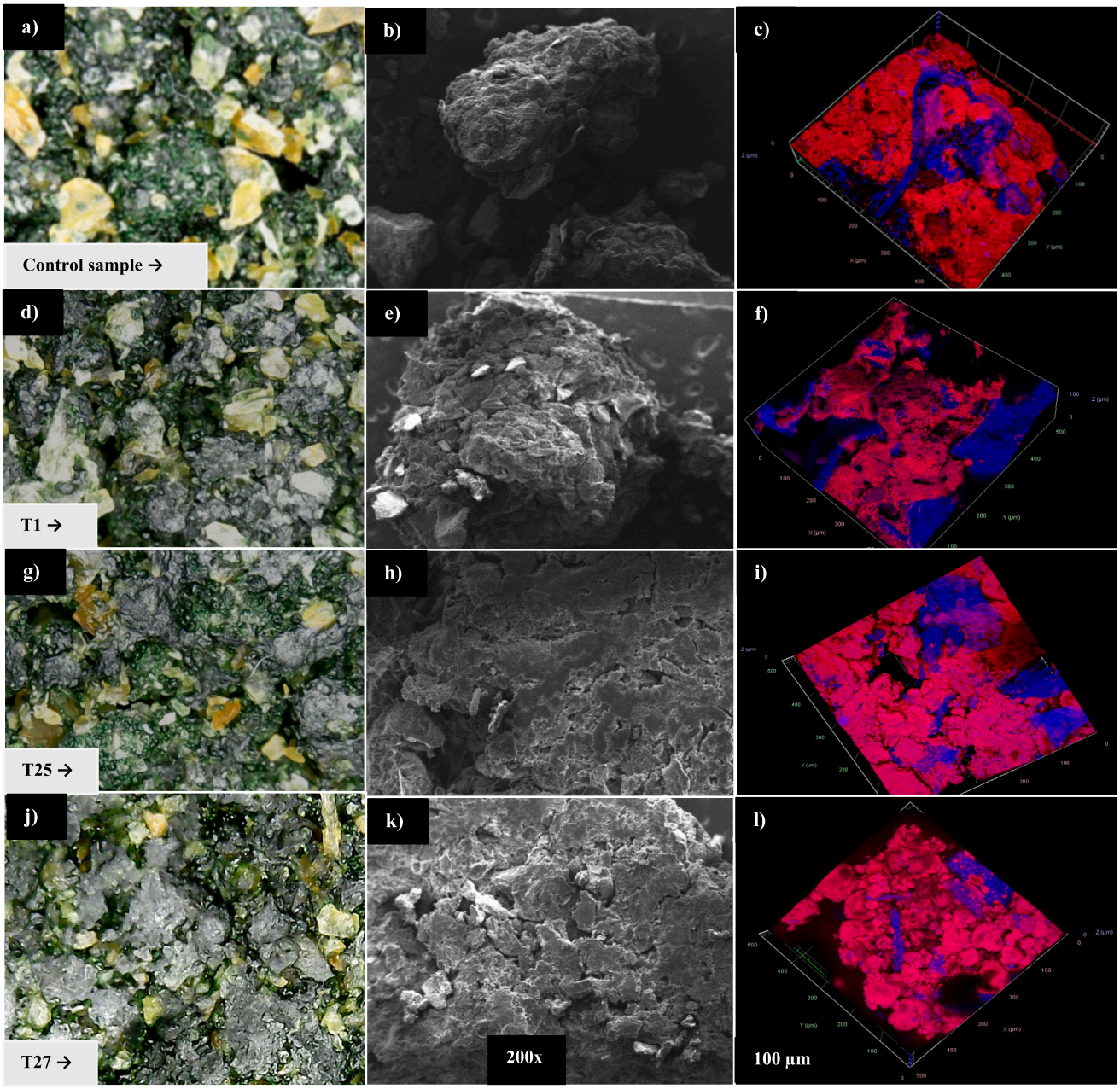


Fig. 5. Images of microstructural changes in the control sample and samples under ultrasonic agglomeration conditions of 70 % power amplitude, time 20 s, and 3 cycles (T1); 90 % power amplitude, time 30 s, and 3 cycles (T25) and 5 cycles (T27). Optical microscopy is shown in a), d), g), and j), scanning electron microscopy in b), e), h), and k), and confocal microscopy in c), f), i), and l).

heterogeneous and less uniform paste. In the present study, synergy between spirulina and cochayuyo flours was observed, given that the flours agglomerated separately, and there was a complete disintegration in the sample with only cochayuyo flour in preliminary tests. In contrast, the spirulina flour agglomerate alone was excessively compacted, but tended to break easily into two or three parts. The combined spirulina and cochayuyo samples had greater adhesion and were more compacted. The greater protein solubility of spirulina flour can explain this phenomenon as compared with cochayuyo flour.

The particle size of the flours also influenced their distribution in the agglomeration. Spirulina flour had a mean particle size distribution of 79.49 ± 2.62 (µm) and cochayuyo flour of 308.89 ± 5.61 (µm). This caused spirulina flour to interact better with the NaCl solution, which is an advantage in functional food applications (Larrosa et al., 2018). The components of the cochayuyo flour, mainly the alginate content together with the soluble fiber and lipids, affected the viscosity and solubility of the flour when agglomerating the samples. However, these larger particles form networks that trap water particles due to US-induced morphological changes in the alginate, which results in more compacted samples with higher fracturability values (Caballero et al., 2021).

4. Conclusions

Ultrasonic agglomeration of protein matrices from cochayuyo and spirulina flours proved to be effective and versatile technology for the development of functional food systems with optimized textural and thermal properties. The process yielded matrices with greater cohesion, homogeneity, and stability, without the need for additives, representing a significant advance toward the production of clean-label foods. This

technology responds to the growing demand from consumers and industry for more natural, sustainable, and healthy products. An increase in the intensity of ultrasonic agglomeration occurred, particularly under conditions of 90 % power amplitude, 30-s exposure, and 5 cycles, resulting in greater matrix compaction, which translated into a significant increase in protein denaturation temperature (up to 139 °C). This thermal effect indicates that proteins require more energy to denature due to the formation of denser and more stable molecular networks, reinforcing the system's thermal resistance. Furthermore, under these optimal conditions, an increase in the elastic modulus of up to 80 % and a more than 50 % increase in the fracturability compared to the control sample was observed, demonstrating a substantial improvement in the firmness and mechanical strength of the matrix. The practical implications for the food industry include the production of clean labels and the development of functional foods through the integration of macro- and microalgal proteins. Along with improved texture and stability, precise control of ultrasonic parameters enables customization of texture and mechanical strength, adapting to different technological and sensory requirements. The focus was on specific ultrasonic parameters (power amplitude, time, and cycles), so exploring other factors, such as frequency or total power, could provide additional information. A unique combination of cochayuyo and spirulina flours was used; extrapolation to other protein sources or mixtures requires validation. Consequently, it is recommended to expand studies to include different combinations of raw materials, explore the scalability of the process, and further explore molecular analysis to validate the observed stabilization and functionality mechanisms. Ultrasonic agglomeration emerges as an alternative to being explored in the food industry, with possible applications in the development of functional and sustainable foods.

CRediT authorship contribution statement

Daniela Rivera-Tobar: Writing – original draft, Visualization, Methodology, Formal analysis, Conceptualization. **Mario Pérez-Won:** Writing – review & editing, Supervision, Resources, Project administration, Funding acquisition. **Erick Jara-Quijada:** Writing – original draft. **Luis González-Cavieres:** Writing – original draft. **Gipsy Tabilo-Munizaga:** Writing – review & editing, Supervision. **Roberto Lemus-Mondaca:** Writing – review & editing. **Fernando Osorio-Lira:** Writing – review & editing.

Declaration of competing interest

The authors declare that they have no known competing financial interests or personal relationships that could have influenced the work reported in this paper.

Acknowledgments

The authors gratefully acknowledge the financial support provided by ANID-Chile through the Advanced Human Capital Formation Program National Doctoral Scholarship 2019 (Folio 21231379). The authors also gratefully acknowledge the financial support of the ANID-FONDECYT project N° 1240735.

Data availability

Data will be made available on request.

References

Ahmed, J., & Kumar, V. (2022). Effect of high-pressure treatment on oscillatory rheology, particle size distribution and microstructure of microalgae Chlorella vulgaris and Arthrospira platensis. *Algal Research, 62*, Article 102617. https://doi.org/10.1016/j.algal.2021.102617

Bai, M., Qin, G., Sun, Z., & Long, G. (2015). Relationship between molecular structure characteristics of feed proteins and protein in vitro digestibility and solubility. *Asian-Australasian Journal of Animal Sciences, 29*(8), 1159. https://doi.org/10.5713/ajas.15.0701

Barba, F. J., Grimi, N., & Vorobiev, E. (2015). New approaches for the use of non-conventional cell disruption technologies to extract potential food additives and nutraceuticals from microalgae. *Food Engineering Reviews, 7*, 45–62. https://doi.org/10.1007/s12393-014-9095-6

Barrett, A., Ahnrud, D., Ziegler, X., & Liu, G. (2018). Ultrasonic agglomeration of model flour systems: Process parameter-product physico-thermal property relationships. *Food Science & Technology, 86*(9), 3868–3883. https://doi.org/10.1111/1750-3841.15850

Barrett, A., Ahnrud, G., Ziegler, D., Liu, X., & Kaletunc, G. (2021). Ultrasonic agglomeration of model flour systems: Process parameter-product physico-thermal property relationships. *Journal of Food Science, 86*(9), 3868–3883. https://doi.org/10.1111/1750-3841.15850

Barrett, A., & Capodieci, R. (2019 Nov). Wheat flour as a model system to study process, effects of sonic agglomeration. A new food compression technique. In *Published, abstracts, presentation at the meeting of the Cereals & Grains Association Fostering Food, Evolution, Denver, CO, U.S.A.*

Baur, F. J., & Ensminger, L. G. (1977). The association of official analytical chemists (AOAC). *Journal of the American Oil Chemists' Society, 54*(4), 171–172.

Benelhadj, S., Douiri, S., Ghouilli, A., Hassen, R., Keshk, S., El-kott, A., Attia, H., & Ghorbel, D. (2023). Extraction of Arthrospira platensis (Spirulina) proteins via Osborne sequential procedure: Structural and functional characterizations. *Journal of Food Composition and Analysis, 115*, Article 104984. https://doi.org/10.1016/j.jfca.2022.104984

Bermúdez-Aguirre, D., Mobbs, T., Barbosa-Cánovas, G., & Feng, E. H. (2011). Ultrasound applications in food processing. In G. Barbosa-Cánovas, & J. Weiss (Eds.), *Ultrasound Technologies for Food and Bioprocessing (pp. 65–105)*. Springer. https://doi.org/10.1007/978-1-4419-7472-3.

Bhargava, N., Mor, R., Kumar, K., & Sharanagat, V. (2021). Advances in application of US in food processing: A review. *Ultrasonics Sonochemistry, 70*, Article 105293. https://doi.org/10.1016/j.ultsonch.2020.105293

Braspaiboon, S., Osiriphun, S., Surawang, S., Jirarattanarangsri, W., Kanha, N., & Laokuldilok, T. (2022). Ultrasound-assisted alkaline extraction of proteins in several algae and their nutritional characteristics. *International Journal of Food Science & Technology, 57*(9), 6143–6154. https://doi.org/10.1111/ijfs.15975

Caballero, E., Flores, A., & Olivares, A. (2021). Sustainable exploitation of macroalgae species from Chilean coast: Characterization and food applications. *Algal Research, 57*, Article 102349. https://doi.org/10.1016/j.algal.2021.102349

Cao, X., Cai, C., Wang, Y., & Zheng, X. (2019). Effects of US processing on physicochemical parameters, antioxidants, and color quality of bayberry juice. *Journal of Food Quality, 2019*, 1–12. https://doi.org/10.1155/2019/7917419

Chen, W., Ma, H., & Wang, Y. (2022). Recent advances in modified food proteins by high intensity ultrasound for enhancing functionality: Potential mechanisms, combination with other methods, equipment innovations and future directions. *Ultrasonics Sonochemistry, 85*, Article 105993. https://doi.org/10.1016/j.ultsonch.2022.105993

Cheng, J., & Cui, L. (2021). Effects of high-intensity ultrasound on the structural, optical, mechanical, and physicochemical properties of pea protein isolate-based edible film. *Ultrasonics Sonochemistry, 80*, Article 105809. https://doi.org/10.1016/j.ultsonch.2021.105809

Covacevich, L., Aguilera, J. M., Moreno, M. C., Brossard, N., & Osorio, F. (2024). Rheological and tribological properties of seaweed powders as thickeners for liquid foods. *Food Hydrocolloids, 154*, Article 110116. https://doi.org/10.1016/j.foodhyd.2024.110116

Eze, O., Chatzifragkou, A., & Charalampopoulos, D. (2022). Properties of protein isolates extracted by ultrasonication from soybean residue (okara). *Food Chemistry, 368*, Article 130837. https://doi.org/10.1016/j.foodchem.2021.130837

Farkas, J., & Mohácsi-Farkas, C. (1996). Application of differential scanning calorimetry in food research and food quality assurance. *Journal of Thermal Analysis and Calorimetry, 47*(6), 1787–1803. https://doi.org/10.1007/bf01980925

Fennema, O. R. (1996). In O. R. Fennema (Ed.), *`water and ice' in food chemistry* (3rd ed., pp. 76–94) Marcel Dekker, Inc.

Gavahian, M., Pallares, N., Al Khawli, F., Ferrer, E., & Barba, F. (2020). Recent advances in the application of innovative food processing technologies for mycotoxins and pesticide reduction in foods. *Trends in Food Science and Technology, 106*, 209–218. https://doi.org/10.1016/j.tifs.2020.09.018

Gordalina, M., Pinheiro, H. M., Mateus, M., da Fonseca, M. M. R., & Cesário, M. T. (2021). Macroalgae as protein sources—a review on protein bioactivity, extraction, purification and characterization. *Applied Sciences, 11*(17), 7969. https://doi.org/10.3390/app11177969

Guadalupi, L. S., Bianco, M., Cataldi, T. R., Ravnsborg, T., Jensen, O. N., & Calvano, C. D. (2025). Ultrasound-assisted protein extraction for deep proteome analysis of Spirulina and Chlorella microalgae. *LWT, 222*, Article 117647. https://doi.org/10.1016/j.lwt.2025.117647

Jackson, M., & Mantsch, H. H. (1995). The use and misuse of FTIR spectroscopy in the determination of protein structure. *Critical Reviews in Biochemistry and Molecular Biology, 30*(2), 95–120. https://doi.org/10.3109/10409239509085140

Khaire, R., Thorat, B., & Gogate, P. (2021). Applications of ultrasound for food preservation and disinfection: A critical review. *Journal of Food Processing and Preservation, 46*(10), 1–25. https://doi.org/10.1111/jfpp.16091

Ladjal-Ettoumi, Y., Douik, L. H., Hamadi, M., Abdullah, J. A. A., Cherifi, Z., Keddar, M. N., & Nazir, A. (2024). Physicochemical and functional properties of spirulina and chlorella proteins obtained by iso-electric precipitation. *Food Biophysics, 19*(2), 439–452. https://doi.org/10.1007/s11483-024-09836-8

Larrosa, A., Camara, Á., Pohndorf, R., da Rocha, S., & Pinto, L. (2018). Physicochemical, biochemical, and thermal properties of Arthrospira (Spirulina) biomass dried in spouted bed at different conditions. *Journal of Applied Phycology, 30*, 1019–1029. https://doi.org/10.1007/s10811-017-1265-5

Lu, Y., Jiang, Y., Liu, J., Yang, X., Zhao, Y., & Fan, F. (2024). Preparation and Properties of Walnut Protein Isolate–Whey Protein Isolate Nanoparticles Stabilizing High Internal Phase Pickering Emulsions. *Foods, 13*(15), 2389. https://doi.org/10.3390/foods13152389

Masavang, S., Roudaut, G., & Champion, D. (2019). Identification of complex glass transition phenomena by DSC in expanded cereal-based food extrudates: Impact of plasticization by water and sucrose. *Journal of Food Engineering, 245*, 43–52. https://doi.org/10.1016/j.jfoodeng.2018.10.008

Mateluna, C., Figueroa, V., Ortiz, J., & Aguilera, J. (2020). Effect of processing on texture and microstructure of the seaweed Durvillaea Antarctica. *Journal of Applied Phycology, 32*(6), 4211–4219. https://doi.org/10.1007/s10811-020-02259-1

Mo, Y. D., Lian, H. S., & Mo, D. Y. (2019). Study on different ultrasound assisted modes, in biomass compression. *International Journal of New Developments in Engineering and, Society, 3*(1). https://doi.org/10.25236/IJNDES.19123

Nilusha, R. A. T., Jayasinghe, J. M. J. K., Perera, O. D. A. N., Perera, P. I. P., & Jayasinghe, C. V. L. (2021). Proximate composition, physicochemical, functional, and antioxidant properties of flours from selected cassava (Manihot esculenta Crantz) varieties. *International Journal of Food Science, 2021*(1), Article 6064545. https://doi.org/10.1155/2021/6064545

Pereira, A. M., Lisboa, C. R., & Costa, J. A. V. (2018). High protein ingredients of microalgal origin: Obtainment and functional properties. *Innovative Food Science & Emerging Technologies, 47*, 187–194. https://doi.org/10.1016/j.ifset.2018.02.015

Pétrier, C., Combet, E., & Mason, T. (2007). Oxygen-induced concurrent ultrasonic degradation of volatile and non-volatile aromatic compounds. *Ultrasonics Sonochemistry, 14*(2), 117–121. https://doi.org/10.1016/j.ultsonch.2006.04.007

Prates, J. A. M. (2025). Unlocking the functional and nutritional potential of microalgae proteins in food systems: A narrative review. *Foods, 14*(9), 1524. https://doi.org/10.3390/foods14091524

Purdi, T., Setiowati, A., & Ningrum, A. (2023). Ultrasound-assisted extraction of spirulina platensis protein: Physicochemical characteristic and techno-functional properties. *Journal of Food Measurement and Characterization, 17*(5), 5474–5486. https://doi.org/10.1007/s11694-023-02051-y

Rahman, M. M., & Lamsal, B. (2021). Ultrasound-assisted extraction and modification of plant-based proteins: Impact on physicochemical, functional, and nutritional properties. *Comprehensive Reviews in Food Science and Food Safety, 20*(2), 1457–1480. https://doi.org/10.1111/1541-4337.12709

Rivera-Tobar, D., Pérez-Won, M., Jara-Quijada, E., González-Cavieres, L., Tabilo-Munizaga, G., & Lemus-Mondaca, R. (2024). Principles of ultrasonic agglomeration and its effect on physicochemical and macro-and microstructural properties of foods. *Food Chemistry*. https://doi.org/10.1016/j.foodchem.2024.141309

Rodríguez De Marco, E., Steffolani, M., Martínez, C., & León, A. (2014). Effects of spirulina biomass on the technological and nutritional quality of bread wheat pasta. *LWT - Food Science and Technology, 58*(1), 102–108. https://doi.org/10.1016/j.lwt.2014.02.054

Rostamabadi, H., Chaudhary, V., Chhikara, N., Sharma, N., Nowacka, M., Demirkesen, I., & Falsafi, S. R. (2023). Ovalbumin, an outstanding food hydrocolloid: Applications, technofunctional attributes, and nutritional facts. *A systematic review. Food Hydrocolloids, 139*, Article 108514. https://doi.org/10.1016/j.foodhyd.2023.108514

Sawle, L., & Ghosh, K. (2011). How do thermophilic proteins and proteomes withstand high temperature? *Biophysical Journal, 101*(1), 217–227. https://doi.org/10.1016/j.bpj.2011.05.059

Shevkani, K., Singh, N., Kaur, A., & Rana, J. (2015). Structural and functional characterization of kidney bean and field pea protein isolates*: A comparative study*. *Food Hydrocolloids, 43*, 679–689. https://doi.org/10.1016/j.foodhyd.2014.07.024

Singla, M., & Sit, N. (2021). Application of ultrasound in combination with other technologies in food processing: A review. *Ultrasonics Sonochemistry, 73*, Article 705506. https://doi.org/10.1016/j.ultsonch.2021.105506

Solomonov, A., Kozell, A., & Shimanovich, U. (2024). Designing multifunctional biomaterials via protein self-assembly. *Angewandte Chemie, 136*(14). https://doi.org/10.1002/ange.202318365

Su, J., & Cavaco-Paulo, A. (2021). Effect of ultrasound on protein functionality. *Ultrasonics Sonochemistry, 76*, Article 105653. https://doi.org/10.1016/j.ultsonch.2021.105653

Sun, X., Ding, L., Zhang, L., Lai, S., & Chen, F. (2023). Interaction mechanisms of peanut protein isolate and high methoxyl pectin with ultrasound treatment: The effect of ultrasound parameters, biopolymer ratio, and pH. *Food Chemistry, 429*, Article 136810. https://doi.org/10.1016/j.foodchem.2023.136810

Thakur, A., Sharma, D., Saini, R., Suhag, R., & Thakur, D. (2024). Cultivating blue food proteins: Innovating next-generation ingredients from macro and microalgae. *Biocatalysis and Agricultural Biotechnology, 60*, Article 103278. https://doi.org/10.1016/j.bcab.2024.103278

Uribe, E., Pardo-Orellana, C., Vega-Gálvez, A., Ah-Hen, K., Pastén, A., García, V., & Aubourg, S. (2020). Effect of drying methods on bioactive compounds, nutritional, antioxidant, and antidiabetic potential of brown alga *Durvillaea Antarctica. Drying Technology, 38*(14), 1915–1928. https://doi.org/10.1080/07373937.2019.1679830

Vela, A. J., Villanueva, M., Li, C., Hamaker, B., & Ronda, F. (2023). Ultrasound treatments of tef [Eragrostis tef (Zucc.) trotter] flour rupture starch α-(1, 4) bonds and fragment amylose with modification of gelatinization properties. *LWT, 174*, Article 114463. https://doi.org/10.1016/j.lwt.2023.114463

Yu, S., Zhang, Y., Ge, Y., Zhang, Y., Sun, T., Jiao, Y., & Zheng, X. (2013). Effects of ultrasound processing on the thermal and retrogradation properties of nonwaxy rice starch. *Journal of Food Process Engineering, 36*(6), 793–802. https://doi.org/10.1111/jfpe.12048

Zeller, M., Hunt, R., Jones, A., & Sharma, S. (2013). Bioplastics and their thermoplastic blends from spirulina and chlorella microalgae. *Journal of Applied Polymer Science, 130*(5), 3263–3275. https://doi.org/10.1002/app.39559

Zeng, Q. H., Wang, J. J., Zhang, Y. H., Song, Y. Q., Liang, J. L., & Zhang, X. W. (2020). Recovery and identification bioactive peptides from protein isolate of Spirulina platensis and their in vitro effectiveness against oxidative stress-induced erythrocyte hemolysis. *Journal of the Science of Food and Agriculture, 100*(9), 3776–3782. https://doi.org/10.1002/jsfa.10408

Zhu, F., & Li, H. (2019). Modification of quinoa flour functionality using ultrasound. *Ultrasonics Sonochemistry, 52*, 305–310. https://doi.org/10.1016/j.ultsonch.2018.11.027